Available online at www.sciencedirect.com
ScienceDirect
Journal of Nuclear Materials 373 (2008) 59–70
journal of nuclear materials
www.elsevier.com/locate/jnucmat

Strain-hardening influence on iodine induced stress corrosion cracking of Zircaloy-4

Marion Fregonese *, Christian Olagnon, Nathalie Godin, Alain Hamel, Thierry Douillard

INSA LYON, MATEIS, L. de Vinci, 69621 Villeurbanne cedex, France

Received 20 October 2006; accepted 26 April 2007

Abstract

The iodine induced stress corrosion cracking (SCC) of recrystallized Zircaloy-4 is first intergranular, and then turns to transgranular propagation, before leading to final ductile rupture. In order to progress in the identification of the factors enhancing transgranular propagation of SCC cracks, the effect of strain-hardening on SCC propagation modes is studied. Fractographic observations by SEM of as-received or pre-strained specimens, submitted to iodine methanol under constant load until rupture, show that strain-hardening enhances transgranular propagation of SCC cracks. This propagation mode is associated with a significant acoustic emission. On the base of these results and metallographic observations and texture measurements, the mechanisms associated with strain-hardening at grain scale and their potential consequences on transgranular initiation and propagation of SCC cracks are discussed.

1. Introduction

Zirconium alloys are used in nuclear power reactors as fuel rod cladding and also as structural material in the reactor core. Under power transient conditions, the fuel rod cladding is susceptible to stress corrosion cracking (SCC), induced by the iodine liberated during the nuclear fission of uranium. On a phenomenological point of view, iodine induced SCC failures of zirconium alloys are described in three steps: localization of iodine attack – intergranular development – transgranular propagation (Fig. 1) [1], before final ductile fracture. The proportions of intergranular to transgranular cracking depend on alloy composition and aggressive iodine environment nature [2]. Transgranular propagation occurs by cleavage-like on basal planes and fluting. It is the result of a competition between a plastic accommodation of the applied strain and the brittle fracture of basal planes by iodine assisted cleavage. For both intergranular and transgranular cracking, an iodine adsorption mechanism along the crack walls and at crack tip may be involved [3,4]. For intergranular crack development, adsorption can be assisted by either a dissolution mechanism or the formation of zirconium iodides [5–7]. On the other hand, for transgranular cracking, some calculations [4], confirmed by ab-initio modeling [8], show that iodine adsorption induces a reduction of the Gibbs surface energy, which affects preferentially the basal plane.

In general, crack velocity depends on environmental parameters such as electrochemical potential, nature and concentration or partial pressure of chemical species, temperature; on metallurgical parameters such as alloy composition, texture, yield strength; and on mechanical parameters such as nature, level and orientation of the applied stress, stress intensity factor, strain rate. For the particular case of iodine induced SCC of zirconium alloys, the critical parameters relative to each of the three steps involved in the cracks development are gathered in Table 1.

As far as transgranular cracking is concerned, the specimen texture appears to be the main controlling parameter for unirradiated Zircaloy-4 [9]. It is quantified by an angular parameter Φ^*, describing the variation in preferential orientation of the *c*-axis in the RT plane (Fig. 2). When

* Corresponding author. Tel.: +33 4 72 43 62 19; fax: +33 4 72 43 87 15.
E-mail address: marion.fregonese@insa-lyon.fr (M. Fregonese).

0022-3115/$ - see front matter © 2007 Elsevier B.V. All rights reserved.
doi:10.1016/j.jnucmat.2007.04.052

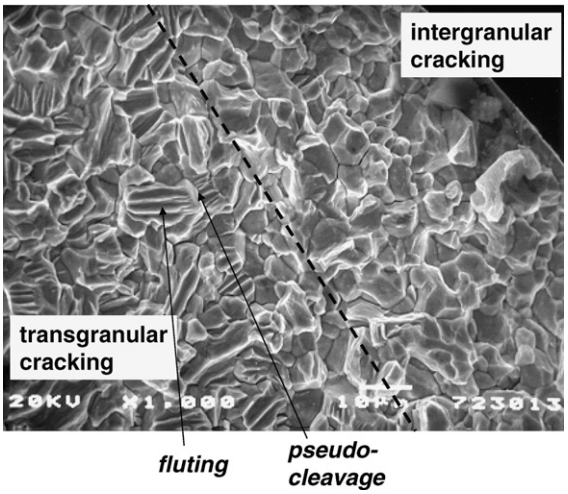

Fig. 1. Intergranular development of SCC cracks, followed by transgranular propagation with cleavage-like and fluting (SSRT on irradiated Zircaloy-4 in a 5×10^{-6} g/g iodine methanol solution at ambient temperature) [1].

the deviation from the preferential *c*-axis orientation is increased towards the radial direction, the threshold value being around 30° [9], transgranular cracking occurs as soon as the stress intensity factor overshoots a threshold value $K_{I\text{-}SCC}$ [6].

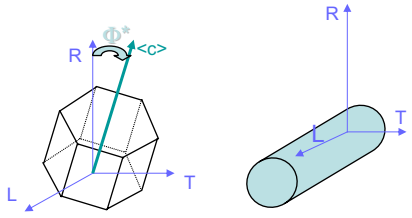

Fig. 2. Definition of angle Φ^*, representative of material texture effect on transgranular cracking (*L*: rolling direction, *T*: transverse direction, *R*: radial or normal direction).

Yet, the effect of strain-hardening on iodine induced stress corrosion cracking of zirconium alloys, in particular on cracks propagation modes, was poorly studied. On the other hand, few studies deal with the use of acoustic emission to monitor zirconium alloys SCC [10,11], whereas this technique is widely used in the particular domain of materials embrittlement by SCC processes [12,13].

In that context, the purpose of that study is to gain insight in the effects of strain-hardening on cracks propagation modes, and more generally in the understanding of the mechanisms involved in SCC cracks development. A strain-hardening pre-treatment is applied on Zircaloy-4 samples. Resulting microstructures are characterized with attention paid to respective activation of twinning and gliding during strain-hardening pre-treatments. Pre-strained or

Table 1
Parameters influencing the different steps of iodine induced SCC of Zircaloy-4

	Initiation	Intergranular development	Transgranular propagation
Environmental parameters	Iodine concentration or partial pressure		
	Oxygen partial pressure		
	Temperature		
Mechanical parameters	Local plastic strain		Stress intensity factor
	Strain rate		
	Stress level and orientation		
Metallurgical parameters	Grain orientation		Texture

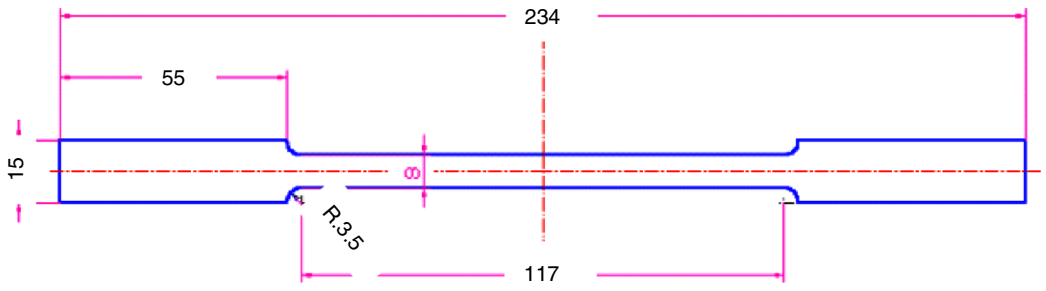

Fig. 3. Tensile specimens shape (dimensions in mm).

Table 2
Composition (Zr: bal.) and mechanical properties (obtained at $d\varepsilon/dt = 10^{-3}\ s^{-1}$) of the studied Zircaloy-4 sheet

Cr	Fe	O	Sn	Al	C	Hf	N	Ni	Si	YS	σ_M	ε_H	A
.11%	.21%	.13%	1.32%	20 ppm	139 ppm	57 ppm	28 ppm	22 ppm	102 ppm	430 MPa	475 MPa	8.5%	20%

YS: 0.2% yield strength, σ_M: plastic instability stress, ε_H: homogeneous strain, A: ductility at failure.

Table 3
Pre-strain values and applied load during SCC tests (% Yield Strength)

Test	A	B	C	D	E	F
Pre-strain	0%	0%	3%	7.5%	8.1%	10.8%
Applied load during SCC tests (%YS)	77	77	77	73	77	73

as-received tensile specimens are tested under so-called 'constant' load, in presence of iodine methanol. Fractographic analysis is carried out by scanning electron microscopy (SEM), and acoustic emission (AE) monitoring of both strain-hardening pre-treatments and 'constant' load tests helps discussing results.

2. Experimental

Transverse tensile test specimens (Fig. 3) were machined out in a 2.6 mm thick rolled sheet of Zircaloy-4 provided by CEZUS, whose composition and mechanical properties are given in Table 2. All specimens were wet ground up to 1200 grit silicon carbide paper. For some of them, a delimited zone of the gauge length ($\Phi = 5$ mm) was mechanically polished with diamond paste down to 6 μm, then electrochemically polished in a 16.7% perchloric acid + 83.3% monobutylic ether solution, in order to reveal the microstructure. They were rinsed in ethanol then stored in desiccators before testing.

Strain-hardening pre-treatments consisted in interrupted tensile tests in air at constant crosshead displacement speeds, which can be assimilated to constant strain rate tests in the explored strain domain, in the range of 4×10^{-5}–$10^{-2}\ s^{-1}$. Pre-treatment experiments were interrupted at given pre-strains (Table 3) and were monitored by acoustic emission, thanks to two piezo-electric transducers fixed at both ends of the gauge length.

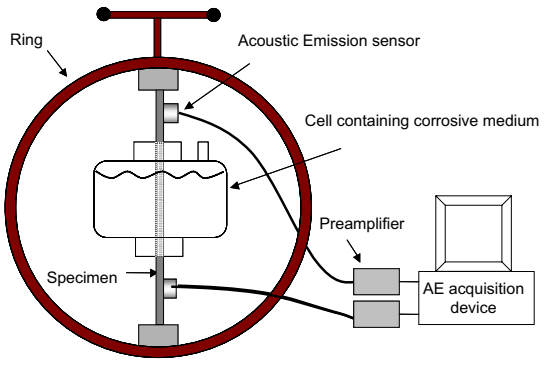

Fig. 4. Experimental device for constant load tests in corrosive medium.

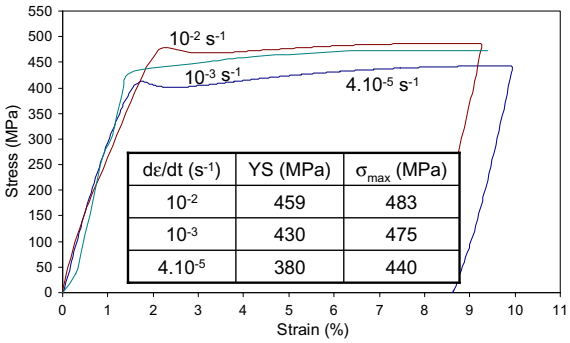

Fig. 5. Stress–strain curves obtained at different strain rates during strain-hardening pre-treatment of the specimens.

Table 4
Maximum stress at interruption of strain-hardening pre-treatment and resulting hardening (load = 1000 g) depending on strain rate

Strain rate (s^{-1})	Maximum stress (MPa)	Hardness (HV)
No	–	202
4×10^{-5}	412	206
10^{-3}	473	235
10^{-2}	479	279

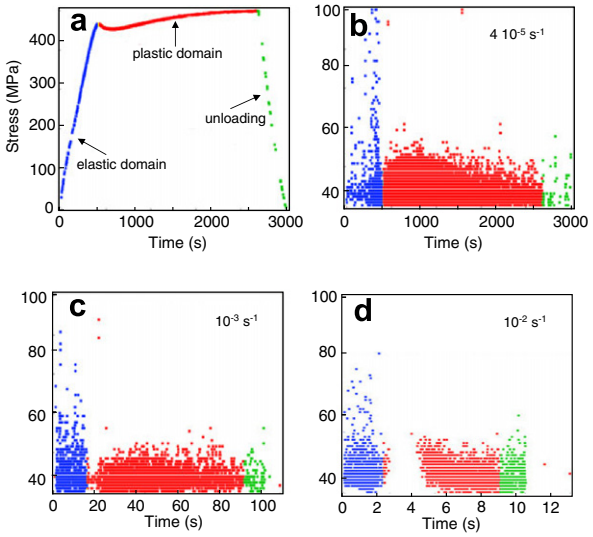

Fig. 6. Acoustic emission recordings during strain-hardening pre-treatment of the specimens: (a) different domains of acoustic activity; (b) amplitude (dB) versus time for $d\varepsilon/dt = 4 \times 10^{-5}\ s^{-1}$; (c) amplitude (dB) versus time for $d\varepsilon/dt = 10^{-3}\ s^{-1}$ and (d) amplitude (dB) versus time for $d\varepsilon/dt = 10^{-2}\ s^{-1}$.

Experimental device for so-called 'constant' load SCC tests is shown in Fig. 4. It consisted in a manually strained tensile ring that induces a stress considered to be constant until SCC cracks develop. Strain gauges fixed on the ring allowed monitoring the stress, in particular after cracking of the specimen. The initial applied stress is expressed in percentage (<100%) of material yield strength (either initial yield strength or maximal stress reached during strain-hardening pre-treatment – Table 2). Aggressive media was contained in a cell and consisted in a 250 mL 10^{-5} g/g iodine methanol solution. AE sensors were fixed on the specimen above and under the experimental cell. As for strain-hardening pre-treatment monitoring, AE sensors consisted in piezo-electric resonant R15D type (from Physical Acoustic Corp.) transducers, linked to pre-amplifiers and Mistras-2001 acquisition device (from PAC). Acquisition threshold was fixed at 25 dB for constant load tests monitoring and was ranged between 35 and 37 dB for pre-treatments tensile tests.

Table 5
Characteristics of acoustic emission recorded during the three domains of strain-hardening pre-treatments, depending on strain rate

Strain rate (s^{-1})		Cumulative energy (arbitrary units)	Acoustic activity	Signals/s
4×10^{-5}	Elastic domain	31079 i.e. 65%	631 signals in 543 s	1.2
	Plastic domain	16451 i.e. 34.4%	26870 signals in 2147 s	12.5
	Unloading	295 i.e. 0.6%	61 signals in 390 s	0.2
10^{-3}	Elastic domain	2378 i.e. 58.6%	707 signals in 15 s	47
	Plastic domain	1652 i.e. 40.7%	3890 signals in 75 s	52
	Unloading	25 i.e. 0.6%	88 signals in 10 s	9
10^{-2}	Elastic domain	8401 i.e. 42.9%	955 signals in 2.3 s	382
	Plastic domain	10908 i.e. 55.7%	2202 signals in 7 s	315
	Unloading	272 i.e. 1.4%	1355 signals in 3.8 s	357

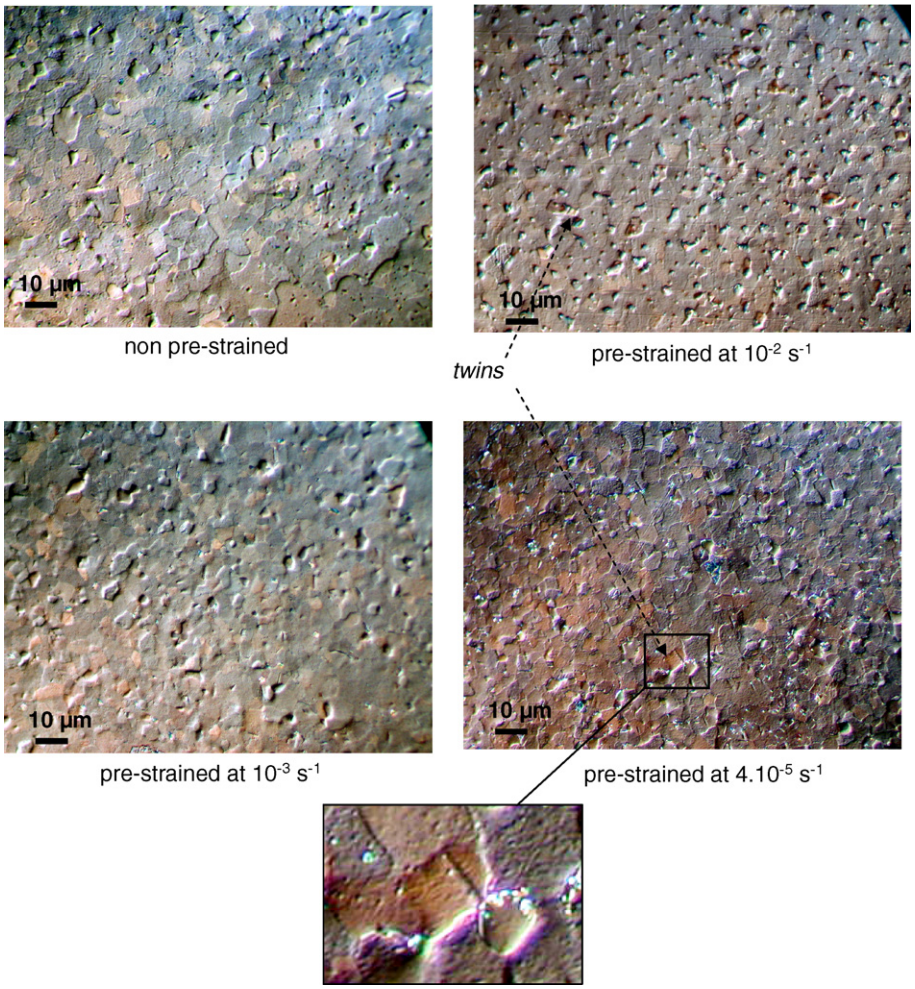

Fig. 7. Microstructures of non-pre-strained and 3% pre-strained specimens at different strain rates (electrolytic polishing was made after tensile test).

3. Results

3.1. Strain-hardening pre-treatment

Fig. 5 gathers the stress–strain curves obtained for specimens pre-treatments carried out at various strain rates, together with hardness measurements (Table 4). As expected, the flow stresses increase with increasing strain rate. Strain rate increase is also associated with an increase of acoustic emission recorded during the test, expressed in terms of number of signals recorded per unit of time (Fig. 6 and Table 5). The three referenced parts of the test are based on the specific deformation domains of the specimen (elastic domain, plastic domain, and unloading) and are associated to also three specific acoustic activity domains. Amplitude and energy of acoustic emission signals recorded during elastic deformation of the specimens are higher than for signals recorded in the plastic deformation domain, for lowest strain rates (4×10^{-5} and $10^{-3}\,s^{-1}$), whereas acoustic emission rate is lower. Yet, the gap in acoustic rate and repartition of cumulative energy between elastic and plastic domains tends to shorten when strain rate increases. At the highest strain rate, acoustic emission rate (nb of signals/s) and repartition of cumulative energy are in the same order of magnitude for both deformation domains. On the other hand, it clearly appears that acoustic rate globally increases with strain rate for the whole test. Correlation between these two parameters is moreover almost linear for the elastic deformation domain. A 'silent' period is recorded just after yielding for the test performed at $10^{-2}\,s^{-1}$, due to Kaiser's effect (no acoustic activity until the applied stress has not yet overshot the maximal stress reached during previous mechanical loading), all the more pronounced than the solicitation is rapid.

Lastly, the microstructure of the specimens was characterized before and after pre-treatment, for the different strain rates (Figs. 7 and 8). Whether electrochemical polishing was performed after or before strain-hardening pre-treatment, only twins or twins plus persistent dislocation bands resulting from glide are respectively observed. Fig. 7 shows typical microstructures obtained by optical microscopy on as-received or on 3% strained specimens at various strain rates, polished after pre-treatment. Only two twins are detected in the observed area, on the $4\times10^{-5}\,s^{-1}$ and $10^{-2}\,s^{-1}$ pre-strained specimens, respectively. No increase of the number of twins is then evidenced on pre-strained specimens. The same result is obtained for 8% strained specimens (Fig. 8(a)), whereas persistent dislocation bands are observed when polishing was performed after the test (Fig. 8(b)).

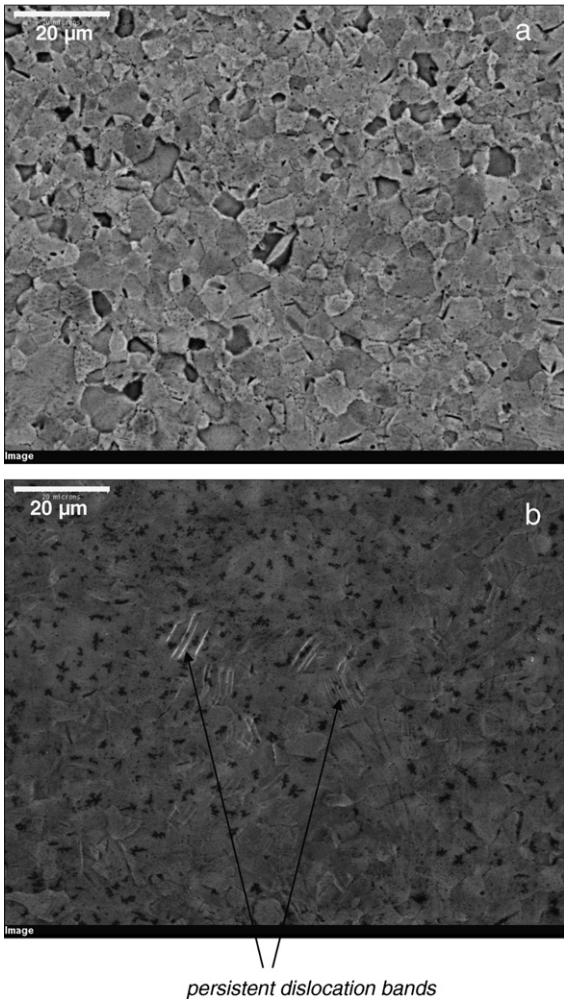

Fig. 8. Microstructures of 8% pre-strained specimens at $10^{-3}\,s^{-1}$: (a) electrolytic polishing was made after tensile test; (b) electrolytic polishing was made before tensile test.

3.2. Influence of strain-hardening on SCC susceptibility

Fig. 9 gathers the results obtained after 'constant' load tests in corrosive medium, for non-pre-strained specimens (tests A and B). The curves give the evolution of applied stress and acoustic emission, expressed in number of cumulative signals, versus time of test. The times to failure of the specimens appear to be very scattered due to the fact that initiation of cracks is not controlled in that kind of experiments performed on non-pre-cracked specimens. For that reason, the curves are focused on a period of 20 000 s including the time of final fracture (i.e. final load decrease to zero). The repartition of different modes of cracking: intergranular (I), transgranular (T), mixed ($M=T+I$) and ductile (D) on fracture surface is also schematized. It is worth noting that transgranular propagation is either limited (test B) or even absent (test A). In these experimental conditions, it appears that transgranular cracking is not the main fracture mode. This result can be explained by texture measurements obtained by electron back scattering diffraction (EBSD). Fig. 10 shows poles repartition in (0 0 1) plane, indicating that c-axis are preferentially inclined towards tangential direction in RT plane (Fig. 2) according to an average 30° angle with R direction, i.e. $\Phi* = 30° \pm 2°$. It corresponds to the threshold value for

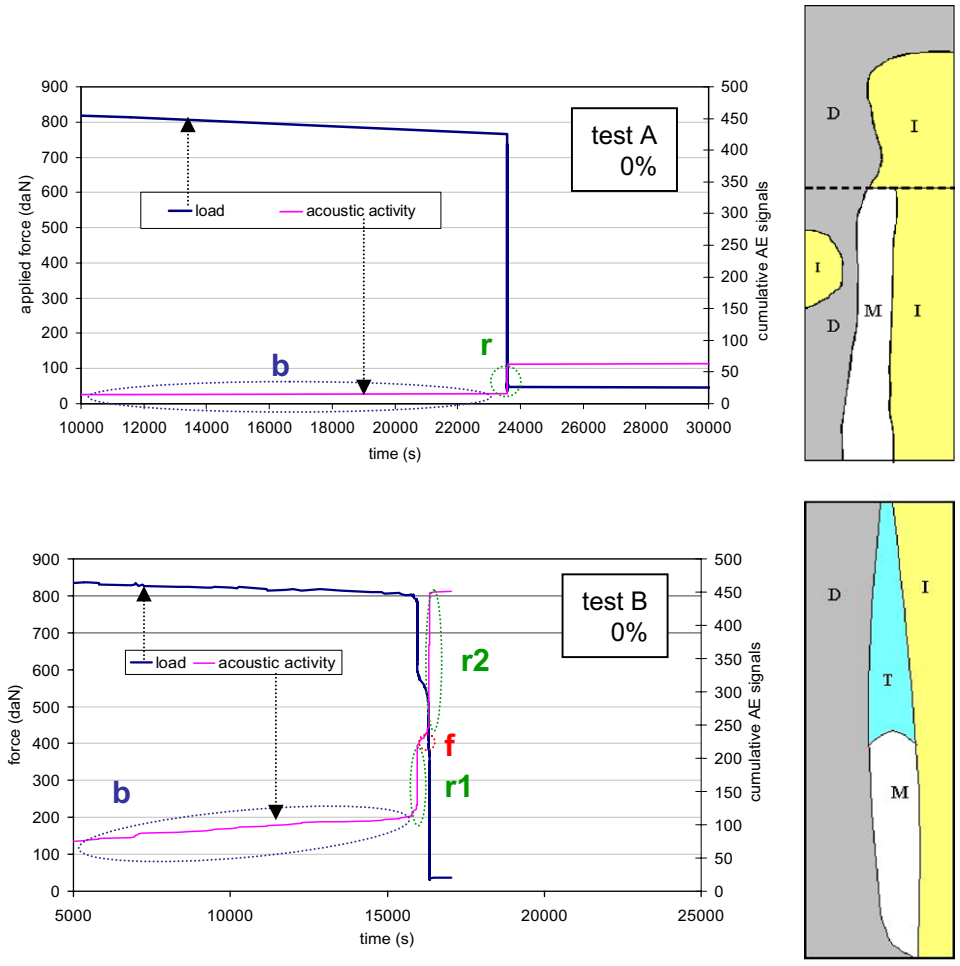

Fig. 9. Evolution of applied load and acoustic activity versus time of test (focused on a 20000 s period around specimen time to failure), and repartition of different cracking modes: intergranular (I), transgranular (T), mixed ($M = I + T$) and ductile (D), on failure surface of *non-pre-strained* specimens, tested under constant load in corrosive medium (10^{-5} g/g iodine methanol).

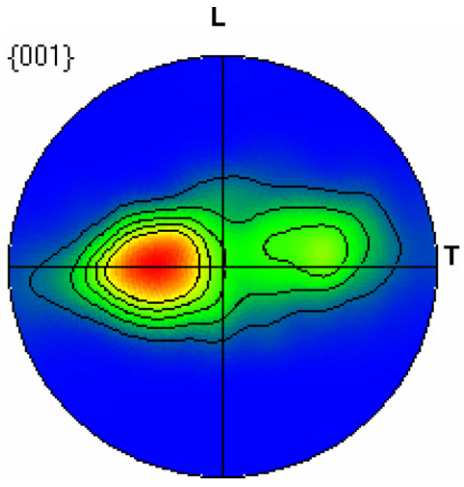

Fig. 10. (001) Pole figure obtained by EBSD for the studied Zircaloy-4 sheet (L: rolling direction, T: transverse direction).

transgranular propagation evidenced in the literature [8]. Therefore, some dispersion in the occurrence of transgranular cracking can exist. The stress evolution during the test shows two main parts: a nearly constant one and another corresponding to an abrupt decrease of stress, corresponding to a sudden, partial or complete, failure of the specimen. These parts are associated with different acoustic emission ratings (Table 6): a rating of relatively low acoustic activity (**b**) and a rating corresponding to a sudden increase in the number of AE signals (**r**), due to elastic energy release linked to partial or final failure of the specimen. For test B, a third step **f** is evidenced, corresponding to a more progressive decrease of stress together with a relative increase of acoustic activity as compared to step **b**.

The results of tests performed on pre-strained specimens, i.e. D, E, F, are presented in Fig. 11. As for as-received specimens, stress remains approximately constant during the first part of the test, indicating that eventually initiated SCC cracks do not propagate. This part is associated with an acoustic activity below 10 signals/h. Fracture parts (**r**) are still associated to a sudden increase of AE signals number. In addition, for all the tests performed

Table 6
Acoustic activity recorded during the different steps of constant load tests in corrosive medium (10^{-5} g/g iodine methanol) for non-pre-strained and pre-strained (at 4×10^{-5} s^{-1}) specimens

Test	Step **b**	Step(s) **f**	
A	2.4 signals/h	–	
B	11.9 signals/h	325 signals/h	
C	–	f1: 12 signals/h	f2: 42 signals/h
D	4.8 signals/h	1220 signals/h	
E	6.8 signals/h	f1: 93 signals/h	f2: 58 signals/h
F	8 signals/h	f1: 208 signals/h	f2: 36 signals/h

on pre-strained specimens, a third part showing a progressive decrease of stress and a high AE rating, ranged between 40 and 1220 signals/h, is evidenced (Table 6). Moreover, for all of these tests, fracture surfaces show some spread transgranular areas, with pseudo-cleavage and fluting (Fig. 11).

The 3% strain-hardened specimen presents a particular SCC behavior (test C). A decrease of stress, associated to SCC cracks development, appeared 24 h after the beginning of the test, and lasted 45 h before final fracture

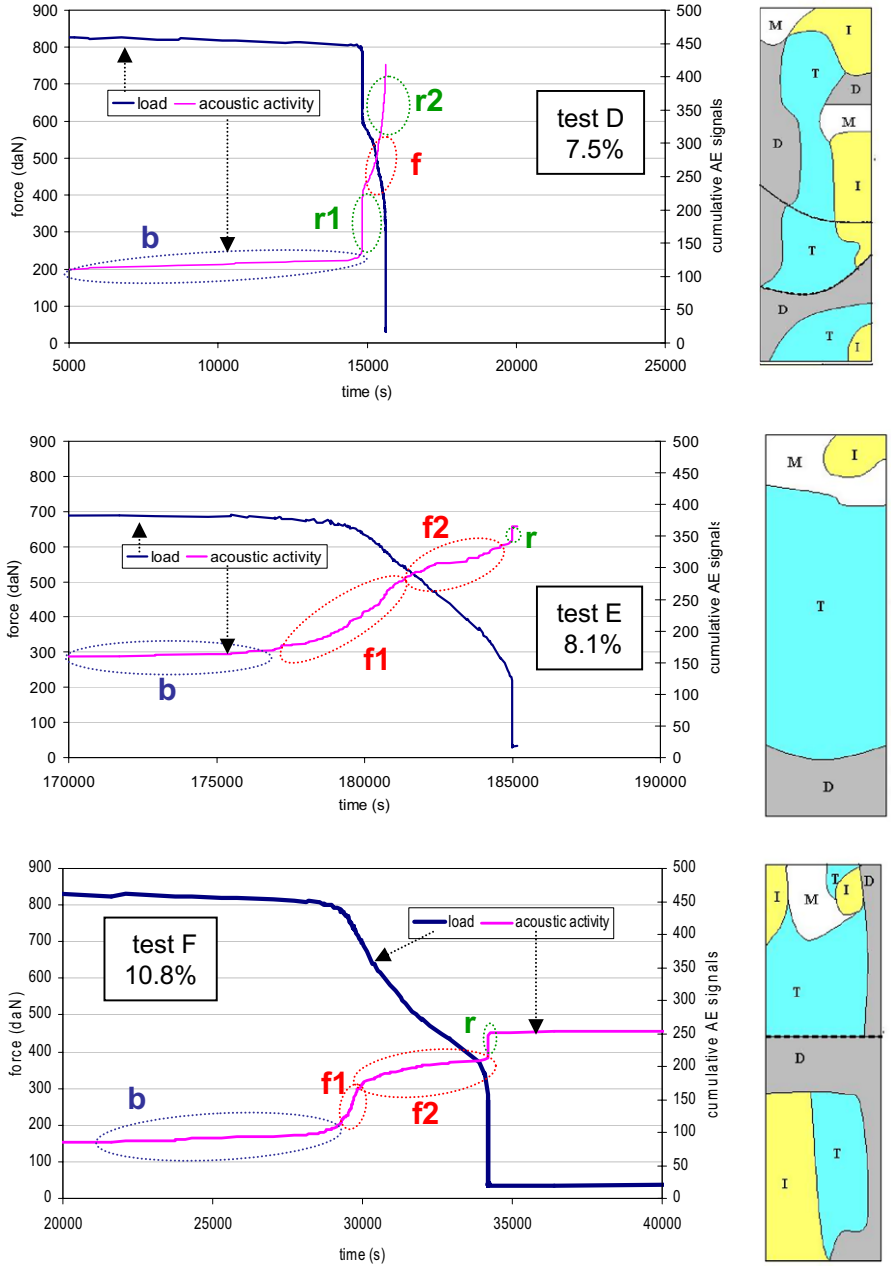

Fig. 11. Evolution of applied load and acoustic activity versus time of test (focused on a 20000 s. period around specimen time to failure), and repartition of different cracking modes: intergranular (*I*), transgranular (*T*), mixed ($M = I + T$) and ductile (*D*), on failure surface of *pre-strained* specimens (at 4×10^{-5} s^{-1}), tested under constant load in corrosive medium (10^{-5} g/g iodine methanol).

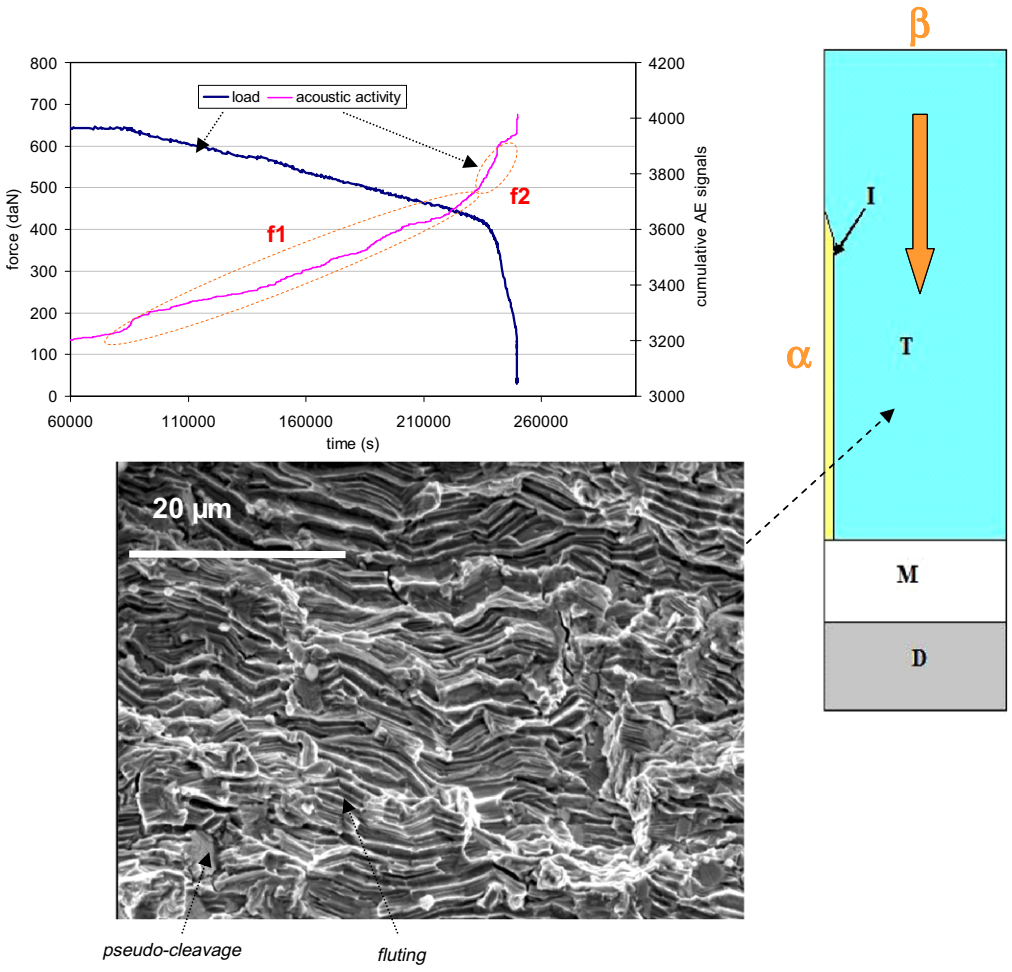

Fig. 12. Evolution of applied load and acoustic activity versus time of test (focused on a 20000 s period around specimen time to failure), and repartition of different cracking modes: intergranular (I), transgranular (T), mixed ($M = I + T$) and ductile (D), on failure surface of the *3% pre-strained* specimen (at 4×10^{-5} s^{-1}), tested under constant load in corrosive medium (10^{-5} g/g iodine methanol).

(Fig. 12). During this crack development stage, two acoustic activities **f1** and **f2**, higher than acoustic activity recorded during part **b**, can be identified. Fracture surface of this specimen presents a spread transgranular area, covering almost 3/4 of the surface rupture. Fluting mainly constitutes the transgranular fracture area. The visual observation of the specimen all along the test allows assessing that the cracks have initiated on α and β faces of the specimen (Fig. 12). The stress decrease, associated with significant acoustic activities (**f1** and **f2**), corresponds to the whole transgranular propagation step before final ductile fracture. Propagation occurred according to the main direction represented by the arrow in Fig. 12.

4. Discussion

The above results show that a progressive decrease of stress, induced by a controlled propagation of SCC cracks, is enhanced by a strain-hardening pre-treatment of the material. It is associated with a transgranular propagation mode of SCC cracks, itself associated to acoustic emission.

This work then evidences that transgranular propagation, consisting in pseudo-cleavage and fluting for Zircaloy-4, is source of acoustic emission, whereas intergranular cracking results in no significant increase of AE, and that strain-hardening enhances transgranular propagation of iodine induced SCC cracks on Zircaloy-4.

4.1. Acoustic emission induced by cracks development

Acoustic emission has been used for several years to monitor SCC phenomena for various metallic materials, as well as to progress in the understanding and the modeling of this particular corrosion mode [12]. Indeed, any structural modification within a material leads to a change in local stress field and then, to energy dissipations, partly released as elastic waves. Every micro-displacement acts then as an acoustic wave emission centre, which propagates up to external surfaces where it is detected. Several mechanisms involved in SCC cracks development are sources of acoustic emission [13]: AE signals are mainly generated by crack initiation and growth. However, the evolution

of hydrogen gas, via cathodic reaction in acid solutions and the breakdown of thick surface oxide film formed under certain circumstances are also important sources of significant AE. In addition, the fracture or decohesion of phases such as precipitates, second phase particles and non-metallic inclusions are expected to produce detectable AE. On the other hand, dissolution of metals can hardly be detected by AE technique. More precisely, the largest AE activity sources during the fatigue-corrosion crack-growth of type 304 L austenitic stainless steels are microcracking processes such as cleavage-like cracking, separations, and intergranular-like cracking [13]. These are caused by the cooperation of triaxial stress (mechanical conditions), corrosive environment (intergranular corrosion or hydrogen evolution), and materials factors (non-metallic inclusions or sensitization). Moreover, for Ti alloys, there exists a good correlation between the SCC crack-growth rate and the detected AE count rate, and the discontinuous character of AE recorded has been associated with a discontinuous cracking, occurring in jumps of some α-grain diameters on a small scale and of a prior β-phase grain diameter on a large scale. For Zr alloys, Cox [10] recorded two types of AE (continuous and discontinuous) during SCC in several media (methanol-1% iodine solution, methanol-1% hydrochloric acid solution and 5% aqueous sodium chloride solutions at room temperature, and fused nitrate–iodide salt mixture at 300 °C). It was then speculated that the continuous type of AE may arise from either electrochemical dissolution processes or the generation of mobile dislocations, whereas the discontinuous type of AE may result from either discontinuous propagation of a brittle crack, twinning of the hexagonal metal, or cracking of the protective oxide at elevated temperatures.

In the present case, when intergranular cracking mainly occurs, i.e. for non-pre-strained specimens, acoustic activity remains relatively low and constant, except when the metal fails. However, AE rate values detected during **b** stages of the performed tests remain higher than those usually evidenced in the same conditions in other works (background of 2 signals/h with a 21 dB threshold for unstressed austenitic stainless steels in de-aerated and de-ionized water [14,15]). This is in agreement with literature results evidencing continuous AE resulting from dissolution processes associated with intergranular cracking [10]. Other authors correlated cracks initiation probability and SCC susceptibility to intermetallic particles present in Zr alloys [16], which is also in agreement with AE associated to cracking. Yet, precipitation is both inter- and transgranular in Zircaloy-4 and no segregation is observed at grain boundaries. Consequently, precipitation can not be the single cause of decohesions, which occur in the present case exclusively at grain boundaries. This is confirmed by the absence of AE signals in situation of stress-assisted intergranular cracking (no more SCC) of Zircaloy-4 tested under high iodine concentration and low stress conditions [17]. The results obtained in the present study are then in agreement with an adsorption–dissolution process involved in intergranular cracking, usually proposed by literature.

As far as transgranular cracking is concerned, literature suggests that cleavage process is at the origin of recorded AE signals in the case of 304 L austenitic stainless steel stress-assisted corrosion [13]. However, cleavage-like planes involved in cfc crystal SCC transgranular cracking (1 1 1) present the same atomic density than those involved in hcp latticed alloys transgranular cracking (basal planes (0 0 1)). It can therefore be suggested that the resulting elastic energy released as acoustic waves within the material is in the same order of magnitude in both cases, and is then responsible for the measured acoustic activity increase. Moreover, fluting is also greatly involved in transgranular cracking processes for Zr alloys and may be also a source of AE, as resulting from prismatic slip accommodating the applied strains. Further analyses of AE signals are necessary to discriminate the one or the other AE source.

4.2. Effects of strain-hardening on cracks propagation modes

The results obtained in the present work evidence that transgranular cracking is enhanced by a strain-hardening pre-treatment of the specimens. Yet, no direct correlation is observed between uniform deformation rate obtained after strain-hardening pre-treatment and percentage of transgranular cracking on surface rupture. Consequently, macroscopic deformation does not seem to be the relevant parameter, but local modifications at grain scale can be responsible for that observation. In order to analyze these results, let's then examine what deformation mechanisms are involved during strain-hardening pre-treatments of the specimens.

Plastic deformation in cubic metals usually operates primarily by slip. Yet, slip systems are not so numerous nor so symmetrically spaced for hcp metals, so that twinning is often competitive with slip. The occurrence of twinning can have consequences on grain orientation and texture which are influent parameters on SCC crack development. Indeed, double twinning process was demonstrated to allow a re-orientation of the basal plane from its original position in the untwinned matrix of Mg–Al alloys [18]. Thus, twinning induced re-orientation of basal planes can be suspected to be at the origin of texture dependant cleavage-like cracking in Zircaloy-4. Twin boundaries have also been identified as an alternate path for iodine induced SCC of zirconium alloys [19].

For hcp polycrystalline zirconium, the incidence of twinning is both temperature and strain rate dependent, more twinning modes becoming active at higher strain rates and lower temperatures [20]. The nature of the activated twinning mode still depends on the stress relative orientation towards basal plane pole. However, at low tensile strain rate ($2.6 \times 10^{-4}\ s^{-1}$) and ambient temperature, the author shows that the twinning shear contribution to the total deformation is only about 15%, and that even in

transverse specimens nearly all the deformation should occur by slip. The present results are in agreement with the latter conclusions, as no increase in the number of twins was observed in the pre-strained specimens. Moreover, AE recordings of strain-hardening pre-treatments support the idea that deformation occurs mainly by slip. Indeed, the dislocation motion produced by deforming polycrystalline metals creates elastic waves large enough to be detected by acoustic emission [21]. However, acoustic emission due to dislocations motion can only be detected for concomitant movements. Furthermore, the packet of dislocations must move far enough and fast enough. Since these conditions are not often simultaneously satisfied, only a small fraction (1%) of dislocation motion associated with plastic flow produces acoustic emission. In that context, higher amplitude and energy of AE signals recorded here during macroscopic elastic deformation of Zircaloy-4 for the lowest strain rates (Fig. 6 and Table 5), compared to the signals recorded during plastic deformation, indicate that, as deformation proceeds, more and more obstacles to the glide of the dislocation packets are produced [20]. These obstacles progressively reduce the distance the dislocation packets move, and thereby reduce the magnitude of the elastic waves produced. This process implies a shift in the distribution of signal amplitudes toward smaller amplitude with increasing strain from the acoustic emission peak observed at the onset of plastic flow. Analogous results were obtained through tensile tests performed on Zircaloy-2: an AE peak was detected for low strains in the elastic flow domain, whereas acoustic activity was quite nil during further deformation of the metal [22]. Yet, according to the present results, it appears that the obstacles to gliding dislocations formed during strain-hardening step are less numerous or more distant when strain rate increases. Indeed, cumulative energy remains high during plastic deformation at high strain rate ($10^{-2}\ s^{-1}$). Consequently, dislocations can glide over relatively long distances during plastic deformation in that latter case. This result is confirmed by the analysis of strain–stress curves obtained at different strain rates (Fig. 5): higher the strain rate, lower the difference between the maximum of stress σ_{max} (at the interruption of the test) and yield strength YS. The evolution of the difference of the percentages of cumulative acoustic energy between the elastic and the plastic domains $\Delta E_{\%el\text{-}pl}$ (see Table 5) with (σ_{max}-YS) is plotted on Fig. 13: a linear correlation is obtained, assessing that acoustic energy dissipation directly results from dislocation gliding.

The AE results obtained here are also in agreement with a low contribution of twinning during deformation. This process is known to result in the emission of high energy and amplitude signals, which are recorded in a weak number in the present experiments.

If twinning is not significantly involved in strain-hardening, the effects on transgranular development of SCC cracks are then linked to dislocation glide. In non-irradiated zirconium alloys after small deformations (1.5–3%) at ambient temperature, the prismatic slip system is the predominant activated slip system [1]. Close to the grain boundaries, other dislocation systems can be observed, corresponding to the pyramidal slip system with principally an $\langle a \rangle$ Burgers vector. The dominant component of the dislocation density is of screw character [1,23]. For higher uniform strain (7–10%), the activation of the pyramidal slip system with $\langle c + a \rangle$ dislocations is enhanced.

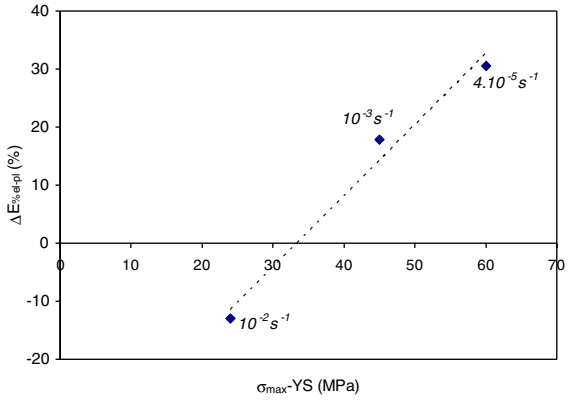

Fig. 13. Evolution of the difference of the percentages of cumulative acoustic energy between the elastic and the plastic domains $\Delta E_{\%el\text{-}pl}$ (see Table 5) with (σ_{max}-YS), for the different strain rates of strain-hardening pre-treatments.

Interactions dislocations/dislocations during further deformation of pre-strained specimens could be responsible for deformation localization occurrence within grains. Indeed, in several SCC mechanisms proposed by the literature [24], corrosion–deformation interactions constitute the driving force for crack propagation. All processes enhancing localization of the deformation within grains could then be susceptible to promote transgranular crack propagation, with embrittlement of dense crystallographic planes. Localization of deformation could also contribute to passive oxide film rupture constituting the first step in SCC cracks development on Zircaloys. It could then be susceptible to enhance transgranular initiation, but also transgranular propagation, as competition between repassivation and iodine adsorption on crack walls and at crack tip is involved in crack development of a passive metal such as zirconium [25]. Yet, Monnet et al. recently demonstrated that the motion of screw dislocations is weakly sensitive to the presence of a prismatic forest. This means that no dislocation annihilation process does occur during further deformation of strain-hardened Zircaloy-4, and that localization of the deformation cannot be at the origin of transgranular cracking enhancement.

Strain incompatibilities between grains has also been proposed by literature to explain the relative occurrence of intergranular and transgranular development of cracks [26]. In that model, intergranular cracks preferentially develop along grain boundaries which are almost normal to the stress axis. When the difference of the crystallographic orientations is large between two adjacent grains, the intergranular crack extension is enhanced by the local stress concentration. On the other hand, transgranular

microcracks initiate preferentially at intersections of coarse slip bands and grain boundaries caused by the stress concentrations induced there. They extend along basal planes into grains less favorably oriented for prismatic slip. Hence, if the basal planes are parallel to the applied stress, the stress will be relaxed by prismatic slip, plastic deformation will occur and the component normal to the basal planes, responsible for iodine induced pseudo-cleavage, will be zero; if instead the basal planes are perpendicular to the stresses the only possible plastic relaxation will be by pyramidal slip at a higher critical resolved shear stress [19], and transgranular cracks can propagate. In the case of the pre-strained material, preferential cracks initiation sites consisting in coarse slip bands and grain boundaries intersections are more numerous, which can enhance transgranular cracks initiation. Moreover, in grains initially well oriented for prismatic slip, further deformation becomes harder due to strain-hardening induced dislocation number increase. Difference of the crystallographic orientations between two adjacent grains effect is then reduced, which is about to limit intergranular development of cracks. On the other hand, transgranular cracking can be enhanced even in grains primarily better oriented for prismatic slip than for pseudo-cleavage on the basal plane, because of strain-hardening induced dislocation number increase within these grains.

Finally, in the case of non-irradiated Zr alloys, a strong Bauschinger effect is reported [27]. This phenomenon can be described on the assumption that the flow stress is the sum of two components: the isotropic stress and the kinematic or internal stress. It is observed that for the unirradiated material, the isotropic stress is nearly constant with plastic strain whereas the internal stress increases with plastic strain, which is in agreement with the fact that the strain-hardening in Zr alloys is mainly due to the increase of the internal stress, whereas the isotropic hardening is low [27]. This phenomenon was attributed to again strain incompatibilities between grains due to the plastic anisotropy of the hcp grains which present a limited number of easy glide slip systems. This increase in internal stress can be responsible for an increase of the stress intensity factor at crack tip, which can reach the threshold value $K_{\text{I-SCC}}$ for transgranular propagation of cracks.

5. Conclusions

This work was aimed at studying the effect of strain-hardening on transgranular cracking during iodine induced SCC of Zircaloy-4, in order to improve the understanding of SCC mechanisms. As-received and pre-strained tensile specimens were tested under so-called constant load in iodine methanol and tests were monitored by acoustic emission.

Conclusions can be given as follows:

- Transgranular propagation of SCC cracks is source of acoustic emission, whereas intergranular development is not associated to a significant increase of acoustic activity; this result is in agreement with the occurrence of an adsorption–dissolution mechanism for intergranular development, whereas transgranular cracking involves brittle fracture of dense crystallographic planes combined with plastic deformation.
- Strain-hardening enhances transgranular propagation of SCC cracks.
- In the present experimental conditions, the contribution of twinning during deformation remains limited; the influence of strain-hardening on transgranular cracking is therefore linked to prismatic slip activation.
- If no strain localization within grains can be responsible for transgranular cracking enhancement, strain incompatibilities between grains can be considered to account for pseudo-cleavage activation on strain-hardened Zircaloy-4; they act at favouring transgranular initiation at coarse slip bands and grain boundaries intersections and increasing the internal stress component of flow stress.

Acknowledgements

The authors thank Annick Elie, Irene Alcazar, Robert Di Folco and Kader Benaziza for their experimental and technical support. The authors are also grateful to CEZUS for providing the material.

References

[1] M. Fregonese, C. Regnard, L. Rouillon, T. Magnin, F. Lefebvre, C. Lemaignan, in: G.P. Sabol, G.D. Moan (Eds.), Zirconium in the Nuclear Industry, Twelfth Conference, ASTM-STP, 1354, American Society for Testing and Materials, 2000, p. 377.
[2] B. Cox, J. Nucl. Mater. 170 (1990) 1.
[3] R.E. Williford, J. Nucl. Mater. 132 (1985) 52.
[4] S.K. Hwang, H.T. Han, J. Nucl. Mater. 161 (1989) 175.
[5] D. Cubicciotti, R.L. Jones, B.C. Syrett, in: D.G. Franklin (Ed.), Zirconium in the Nuclear Industry, Fifth Conference, ASTM-STP, 754, American Society for Testing and Materials, 1982, p. 146.
[6] B. Cox, J.C. Wood, in: P.R. Swann, F.P. Ford, A.R. Westwood (Eds.), Proceedings of the Conference of Mechanisms of Environment Sensitive Cracking of Materials, Metals Society of London, Guilford (UK), 1977, p. 520.
[7] D. Cubicciotti, A.C. Scott, J. Less Common Met. 77 (1981) 241.
[8] A. Legris, C. Domain, Philos. Mag. 85 (2005) 589.
[9] I. Schuster, C. Lemaignan, J. Nucl. Mater. 189 (1992) 157.
[10] B. Cox, Corrosion 6 (1974) 191.
[11] S.A. Nikulin, V.G. Khanzhin, A.B. Rojnov, Corrosion Nace 2002, Paper No. 02437.
[12] H. Mazille, R. Rothea, in: K.R. Tretheway, P.R. Roberge (Eds.), Modeling Aqueous Solutions, Kluwer Academic, Netherlands, 1994, p. 103.
[13] S. Yuyama, T. Kishi, Y. Hisamatsu, J. Acoustic Emission 2 (1983) 71.
[14] M. Fregonese, H. Idrissi, H. Mazille, L. Renaud, Y. Cetre, Corros. Sci. 43 (2001) 627.
[15] Y.P. Kim, M. Fregonese, H. Mazille, D. Feron, G. Santarini, Corros. Eng. Sci. Tech. 40 (2005) 301.
[16] T. Kubo, Y. Wakashima, M. Imahashi, J. Nucl. Mater. 132 (1985) 126.

[17] E. Munch, L. Duisabeau, M. Fregonese, H. Mazille, L. Fournier, in: Proceedings of Eurocorr 2004, Nice, France, 2004.
[18] L. Jiang, J.J. Jonas, A.A. Luo, A.K. Sachdev, S. Goget, Scripta Mater. 54 (2006) 771.
[19] R.E. Haddad, A.O. Dorado, in: A.M. Garde, E.R. Bradley (Eds.), Zirconium in the Nuclear Industry, Tenth Conference, ASTM-STP, 1245, American Society for Testing and Materials, 1994, p. 559.
[20] R.E. Reed-Hill, Role of deformation twinning in the plastic deformation of a polycrystalline anisotropic metal, in: R.E. Reed-Hill, J.P. Rosi, H.C. Rogers, (Eds.), Deformation Twinning, vol. 25, 1964, p. 295.
[21] C.R. Heiple, S.H. Carpenter, J. Acoustic Emission 6 (1987) 177.
[22] P.K. Chaurasia, C.K. Mukhopadhyay, S. Murugan, P. Muralidharan, K. Chandran, V. Ganesan, T. Jayakumar, P.V. Kumar, J. Nucl. Mater. 322 (2003) 217.
[23] G. Monnet, B. Devincre, L.P. Kubin, Acta Mater. 52 (2004) 4317.
[24] T. Magnin, A unified model for trans and intergranular stress corrosion cracking, in: T. Magnin, J.M. Gras (Eds.), Corrosion–Deformation Interactions, Les éditions de physique, 1993, p. 27.
[25] J.C. Wood, J. Nucl. Mater. 45 (1972) 105.
[26] T. Kubo, Y. Wakashima, K. Amano, M. Nagai, J. Nucl. Mater. 132 (1985) 1.
[27] F. Onimus, J.L. Béchade, C. Duguay, D. Gilbon, P. Pilvin, J. Nucl. Mater. 358 (2006) 176.